On the photorelease of nitric oxide by nitrobenzene derivatives; a CASPT2//CASSCF model

Angelo Giussani[*,‡] and Graham A. Worth[†]

[‡]Instituto de Ciencia Molecular, Universitat de València, Apartado22085, ES-46071 Valencia, Spain
[†]Department of Chemistry, University College London, 20 Gordon Street, London WC1H 0AJ, U.K.
[*]To whom correspondence should be addressed. Email: Angelo.Giussani@uv.es

Abstract

Nitroaromatics compounds can photorelease NO after UV absorption. The efficiency of the photoreaction depends on the molecular structure and two features have been pointed out as particularly important for the yield of the process: the presence of methyl groups at the ortho position with respect to the nitro group and the degree of conjugation of the molecule. In the present contribution we provide a theoretical characterization at the CASPT2//CASSCF level of thoery of the photorelease of NO for four molecules derived from nitrobenzene through the addition of ortho methyl groups and/or the elongation of the conjugation. Our previously described mechanism obtained for the photorelease of NO in nitrobenzene has been adopted as a model for the process. According to this model, the process proceeds through a reactive singlet-triplet crossing (STC) region that the system can reach from the triplet $^3(\pi o\pi^*)$ minimum. The energy barrier that must be surmounted in order to populate the reactive STC can be associated with the efficiency of the photoreaction. The here obtained results display clear differences for the efficiency of the photoreaction in the studied systems, and can be correlated with experimental results. The model thus proves its ability to highlight differences in the photoreaction efficiency for the nitroaromatic compounds studied here.

1. INTRODUCTION

Among the various fields in which nitroaromatic compounds play an important role, which include the study of atmospheric pollutants and energetic materials,[1,2] a particular interest is found in the drug delivery sector.[3] Nitroaromatics compounds are employed here due to their ability to photorelease nitric oxide (NO), which has various physiological effects useful for the treatment of pathological conditions.[4] The ability to deliver NO as a result of the interaction of light is particularly attractive since it makes it possible to control the release of NO with a precise spatiotemporal resolution.[5]

In order to design the most suitable nitroaromatic compounds for their applications in the drug delivery sector, it is fundamental to understand the molecular basis behind the photodegradation mechanism leading to the formation of NO. The mechanism has been the subject of various experimental and theoretical works,[6–16] from which a scenario has emerged. It is in general accepted that the photoreaction occurs via a photoisomerization of the nitro into a nitrite group, from which NO is subsequently formed. Following the original nomenclature proposed by Chapman et al.,[17] the photoisomerization occurs according to a so-called "intramolecular rearrangement mechanism", in which the key step is the formation of an intermediate in which an oxaziridine ring structure is formed. Such an oxaziridine ring structure has been identified at the CASPT2//CASSCF level for the molecules nitrobenzene and nitronaphthalene as a singlet-triplet crossing region which can lead the population of the triplet excited states back to the ground singlet state and on towards NO formation.[11,12] This mechanism consequently explains the photoreaction as a process passing through the population of the triplet states of the systems with subsequent decay through a reactive STC back to the ground state toward NO formation (see figures 9 and 9a in references 11 and 12, respectively).

In the seminal work of Chapman et al., a second possible photoisomerization mechanism called the "dissociation−recombination mechanism" was proposed, according to which the photoisomerization proceeds via the dissociation of the nitro group from the aromatic ring, followed by its recombination with the aromatic ring giving rise to the nitrite isomer. This mechanism has been theoretically characterized for nitrobenzene, and associated with the so-called roaming mechanism that Suits and co-workers proposed for the nitrobenzene nitro-to-nitrite photoisomerization.[10,15]

Once the general principles of the photomechanism are known, the next step will be the understanding of the fine details that regulate the efficiency of the process. In order to reach such a goal, comparative studies of series of nitroaromatics compounds whose structures present small but clear differences are particularly useful, so as to observe the effect that each structural modification has on the photochemical process.[14] A study of this type was presented by Miyata and co-workers, who experimentally evaluated the photoformation of NO for a series of nitrobenzene derivatives which release NO to form a paramagnetic compound whose ESR signal can be experimentally measured.[4]

In the series of compounds studied by Miyata and co-workers, two types of structural modifications have been analyzed. The first modification is the presence of two methyl groups at ortho positions with respect to the nitro group. An analysis of the effect of such substitution is particularly interesting since it is normally accepted that the presence of ortho methyl groups force the nitro group to adopt a perpendicular orientation with respect to the plane of the aromatic ring, predisposing the geometry to the formation of an oxaziridine ring which favors the photorelease of NO, although a precise theoretical rationalization of this effect has not yet been given as far as we know.[5] The second modification is the extension of the π-conjugation. Having a larger π-electron conjugation will in general lower the ππ* states of the system, making the excited states of the molecule more accessible at lower excitation energies, and consequently resulting in a system more prone to photoreactions.

In this contribution we present a comparative study of the photoinduced mechanism leading to NO formation for the series of nitrobenzene derivatives shown in Figure 1: nitrobenzene (molecule A), 1,3-dimethyl-2-nitrobenzene (molecule B), 1-nitro-4-[(1E)-2-phenylethenyl]benzene (molecule C), 1,3-dimethyl-2-nitro-5-[(1E)-2-phenylethenyl]benzene (molecule D). From the results on these molecules a fifth nitrocompound, 1,3-dimethyl-2-nitro-5-[(1E,3E)-4-phenylbuta-1,3-dien-1-yl]benzene (molecule E) was also selectively characterized. The study has been performed by means of CASPT2//CASSCF calculations, and assuming that the mechanism we have previously theoretically characterized for loss of NO in nitrobenzene and nitronaphthalene is the main one responsible for the NO formation in the molecules studied here. In this mechanism the decay is from the triplet $^3(\pi o\pi^*)$ minimum towards a reactive STC minimum, and the energetic position of these two critical points can be related to the efficiency of the photodegradation.[11,12,15] Key for this work was the characterization of these structures to obtain the energy that separates them.

The selection of these systems has been dictated for the following reasons. Nitrobenzene, molecule A, is the most simple nitroaromatic compound, and is here taken as a reference. Molecules B and C allow the analysis of the effect on the photochemistry of nitrobenzene of the addition of methyl groups at ortho positions and the extension of the π-conjugation, respectively. Molecule D again can provide information on the effect of the presence of methyl groups, comparing its behavior with respect to molecule C, and its ability to photorelease NO was actually detected in the work of Miyata and co-workers. Molecule E is the one among the systems experimentally studied by Miyata and co-workers that photoreleases the most NO.[4] Last but not least, the size of the chosen systems still allows their description at the CASPT2//CASSCF level with an acceptable computational effort.

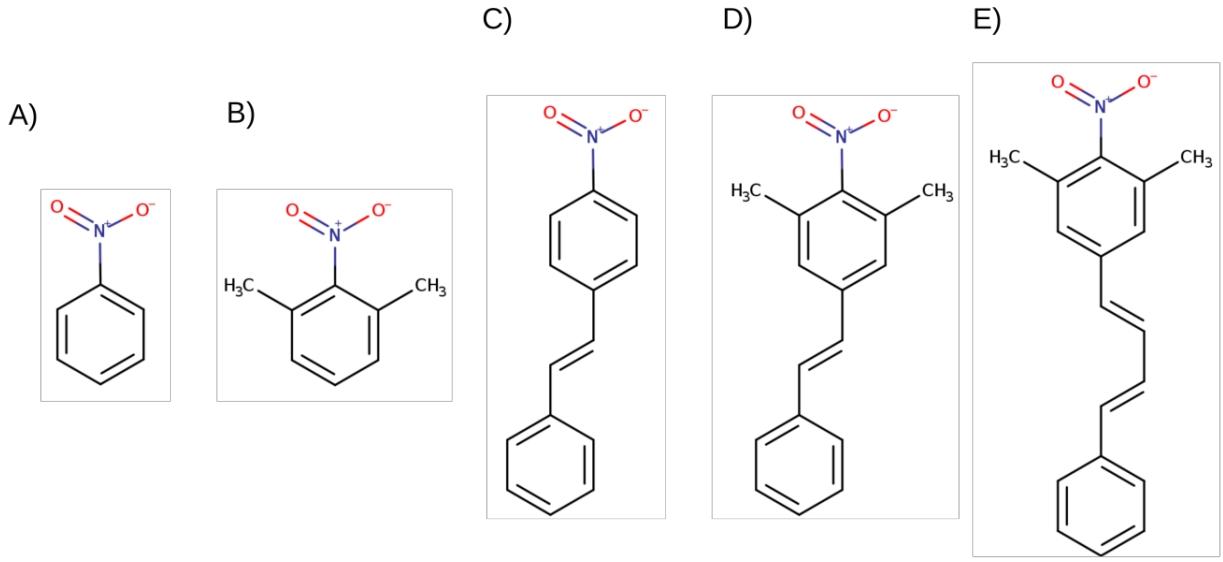

Figure 1. Molecular structure of the nitroaromatic compounds here studied. From left to right: nitrobenzene (molecule A), 1,3-dimethyl-2-nitrobenzene (molecule B), 1-nitro-4-[(1E)-2-phenylethenyl]benzene (molecule C), 1,3-dimethyl-2-nitro-5-[(1E)-2-phenylethenyl]benzene (molecule D), 1,3-dimethyl-2-nitro-5-[(1E,3E)-4-phenylbuta-1,3-dien-1-yl]benzene (molecule E).

2. METHODS

The present study was performed employing a CASPT2//CASSCF approach,[18] i.e. geometry optimizations were performed at the CASSCF level,[19] while final energies were computed at the CASPT2 level.[20] As an exception, ground state optimizations were performed using the MP2 method.[21] No restrictions to the symmetry of the molecules were imposed (C1 symmetry). The basis set of atomic natural orbitals (ANO) of S-type contracted to C,N [4s,3p,1d]/H[2s1p] was employed.[22,23]
As described in detail in the result section, different active spaces have been employed depending on the type of calculation, either CASSCF optimizations or CASPT2 vertical calculations, and the size of the system. In summary, molecules A and B were described at the CASPT2(14,11)//CASSCF(10,8) and at the CASPT2(8,8)//CASSCF(8,8) level, while molecules C and D were studied at the CASPT2(18,15)//CASSCF(14,12) and at the CASPT2(12,12)//CASSCF(12,12) level, while molecule E, the largest of the here studied systems, was treated at the CASPT2(14,14)//CASSCF(14,14) level.

All calculations were performed with the OpenMolcas software.[24] Within the CASPT2 calculations, an imaginary level-shift correction of 0.2 au was used in order to minimize the effects of possible intruder states.[25] The CASPT2 standard zeroth-order Hamiltonian was used as originally implemented and the core orbitals were frozen in the CASPT2 calculations. Cholesky decomposition was used to speed up the calculation of two-electron integrals.[26]

Singlet-triplet crossing regions were computed by using the restricted Lagrange multipliers technique as included in OpenMolcas, in which the lowest-energy point is obtained under the restriction of

degeneracy between the two considered states.[27] Spin-orbit couplings, SOCs, were calculated as described elsewhere.[28] The character of the obtained minima was analyzed by computing the frequencies.

3. RESULTS AND DISCUSSIONS

3.1 Definition of a common active space to describe the four nitroaromatic compounds A-D

The present study aims at a description of the same photoreactive model for the four systems A-D presented in Figure 1, so as to characterize the differences in the process due to the increasing complexity of the original system (molecule A, i.e. nitrobenzene). It is thus fundamental to employ the same level of theory to perform such a characterization, so as to ensure that the obtained results reflect the different properties of the four compounds and are not instead imputable to methodological issues.

A first guess for the active space selection for the description of molecules C and D is to enlarged the CAS(14,11) space previously used for nitrobenzene so to account for the enlarge π system present in these molecules.[12] A reasonable choice is to include the π and π* orbitals of the additional CC double bond and the highest and lowest π and π* orbitals localized on the phenyl group. This results in a CAS(18,15) active space, that, although feasible for single point calculations, is not computationally convenient for geometry optimizations. For that reason we evaluated the possibility of reducing the original CAS(14,11) to a CAS(10,8) space in order to perform geometry optimizations, which seems reasonable taking into account that in the present work we are interested in the description of only the two lowest singlet and triplet states. In order to test such a procedure, we have calculated the critical points forming the adopted model in nitrobenzene at the CASPT2(14,11)//CASSCF(10,8) level, and compared the results with the CASPT2(14,11)//CASSCF(14,11) data. Such a comparison is in order also taking into account the particularly challenging electronic structure of nitrobenzene, proved to be quite sensitive to the adopted computational details.[12,29,30]

Table 1. CASPT2(14,11) energies (eV) of the low-lying singlet and triplet states of molecule A at the optimized geometries at the CASSCF(14,11) and CASSCF(10,8) level.[a]

	molecule A					
	CASPT2(14,11)//CASSCF(14,11)			CASPT2(14,11)//CASSCF(10,8)		
State Geometry	gs	$^3(\pi_O\pi^*)$	$^3(n_A\pi^*)$	gs	$^3(\pi_O\pi^*)$	$^3(n_A\pi^*)$
$^1(gs)_{min}$[b]	0.00	3.40	3.35	0.00	3.40	3.35
$^3(n_A\pi^*)_{min}$	0.73	3.04	2.82	0.71	3.04	2.88
$^3(\pi_O\pi^*)_{min}$	1.10	**2.95**	2.85	1.08	**2.97**	2.87
$(T1/S0)_{mecp}$	3.76	**3.76**	3.94	3.67	**3.70**	4.21

[a] All the reported values refer to the corresponding ground state optimized geometry, $^1(gs)_{min}$.
[b] The ground state geometry, $^1(gs)_{min}$, was optimized at the MP2 level.

From the CAS(14,11) space the H-6, H-5, and L+3 orbitals have been excluded to form the CAS(10,8) space (see Figure S1 in the SI). The adopted exclusion criteria was based on their occupation number for the S0, S1, T1, and T2, states, being in all cases either greater than 1.95 or lower than 0.05. In Table 1, the CASPT2(14,11) energies of two lowest singlet and triplet state of nitrobenzene are reported, calculated at the CASSCF(14,11) and CASSCF(10,8) optimized critical points. The corresponding geometries are depicted in Figure S2 of the SI. Comparing the energies and structures obtained in the two set of computations, is possible to conclude that the CASPT2(14,11)//CASSCF(10,8) protocol

provides a similar scenario to the CASPT2(14,11)//CASSCF(14,11). In particular, the energy difference between the $^3(\pi_O\pi^*)$ minimum and the reactive STC is equal to 0.81 and 0.73 eV, respectively. On the basis of such results, we decided to characterize molecules A and B at the CASPT2(14,11)//CASSCF(10,8) level, while molecules C and D at the CASPT2(18,15)//CASSCF(14,12), which corresponds to the same active space of molecules A and B, plus the 2 π and 2 π^* orbitals on the enlarged π system (see Figure S3 in the SI). In such a way all four systems are described by the same active orbitals localized on the nitrobenzene group, and the more important orbitals describing the enlarged π system of molecule C and D are also accounted for.

3.2 Characterization of the ground state minima and lowest singlet and triplet excited states

Accordingly to our previous experience with nitrobenzene the inclusion of dynamic correlation appears to be important in the optimization of its ground state structure, as the comparison between CASSCF and CASPT2 S0 minima with experimental electron diffraction measurements has shown.[12,31] Due to the high computational cost that CASPT2 optimizations will require for molecules C and D, we resorted to performing ground state MP2 minimization. The comparison of the MP2, the CASPT2(14,11), and the experimental structure of nitrobenzene validates the adopted methodology (see Figure S4 in the SI).

The obtained S0 minima, hereafter indicated as $^1(gs)_{min}$, are reported in Figure 2. The molecular structure shared for all four systems (i.e. the nitro group and the phenyl ring directly attached to it) display similar bond lengths in the four minima. The main geometrical difference that can be appreciated is related to the orientation of the nitro group with respect to the plane of the aromatic ring. While for molecules A and C the plane passing through the nitro group is parallel to the plane of the aromatic ring (making molecules A and C planar), for molecules B and D the nitro group is placed perpendicular with respect to the plane of the aromatic ring. This is a clear consequence of the presence of the methyl groups in molecules B and D. Frequencies calculations were performed at the four minima. Only the S0 minimum of molecule A presents no imaginary frequencies, while the others display small imaginary values, related in molecules B and D to the rotation of the methyl groups, and associated in molecule C and D to the torsion of the second phenyl ring.

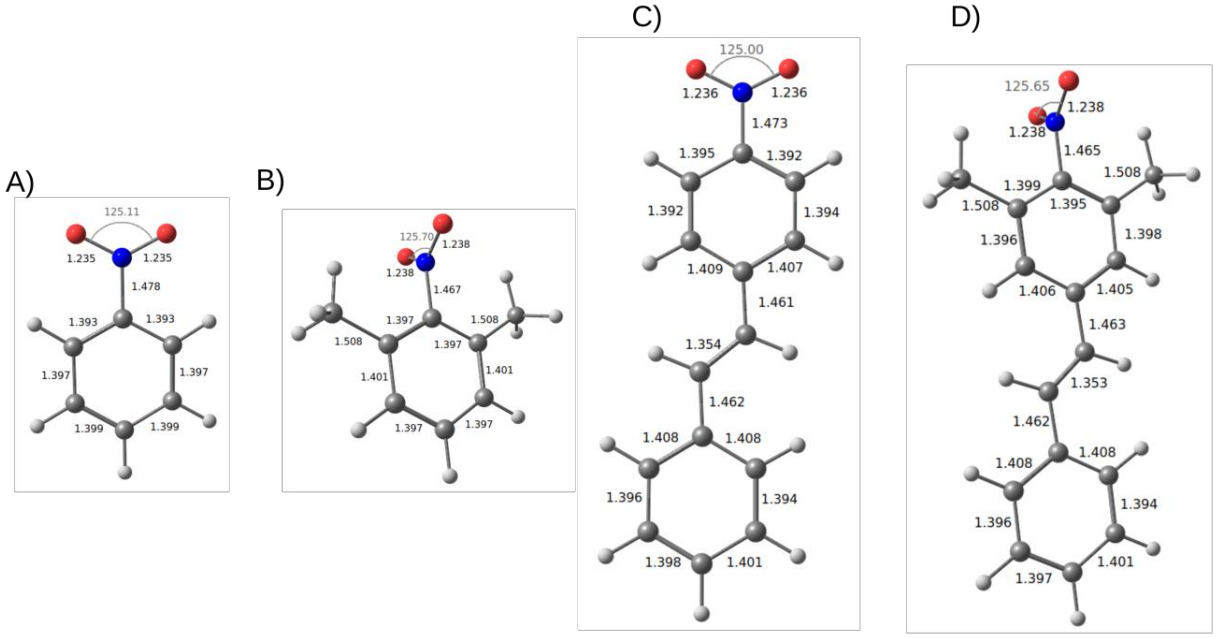

Figure 2. Ground state minima, $^{1}(gs)_{min}$, obtained at the MP2 level for molecules A-D. Selected bond lengths (in Å) and angles (in degrees) are also reported.

At the obtained ground state minima, the low-lying singlet and triplet excited states of the system have been characterized computing six singlet and six triplet electronic states at the CASPT2(14,11) level for molecules A and B, and at the CASPT2(18,15) level for molecules C and D. The so obtained CASPT2 vertical excitation energies, together with the CASSCF oscillator strength associated with the possible transition form the ground state to the singlet excited states, are reported in Table 2. In this Table, an energy-ordering nomenclature has been adopted for the electronic states, while only in particular cases, when the analysis of the corresponding CASSCF wave-function allowed it, the nomenclature based on the particular nature of the state and established in the literature has been used.[12]

Looking at Table 2, both similarities and differences among the four molecules can be observed. In all cases the S_1 state is the $^{1}(n_A\pi^*)$, and the triplet $^{3}(\pi_O\pi^*)$ state is close in energy to it. The latter fact, together with a high SOC between the two states, is the reason behind the high triplet quantum yield observed for nitroaromatics systems.[32–34] Since the photodegradation model that we are adopting here assumes the population of the triplet states, the SOC between the $^{1}(n_A\pi^*)$ and $^{3}(\pi_O\pi^*)$ states at the computed $^{1}(gs)_{min}$ minima have been computed in order to validate the hypothesis of an efficient population of the triplet manifold. The obtained SOC, equal to 74.40, 75.29, 74.53 and 74.60 cm^{-1} respectively, indeed support such an intersystem crossing. Also, the nature of the S_2 state is the same for the four systems, and corresponds to the $^{1}(n_B\pi^*)$ state. It is also interesting to note that molecules A and C display states with a significant oscillator strength among the five singlet excited states computed here, while the states of molecules B and D are significantly darker. This implies that at lower excitation energies, the excited states of molecules A and C will be more easily populated than the excited states of B and D, a fact that will have an impact on the photochemistry of these systems.

Table 2. Vertical excitation energies (E_{VA}, eV) at the MP2 ground-state minima, $^1(gs)_{min}$, for the lowest valence singlet and spin forbidden triplet excited states.[a] Energies computed at the CASPT2(14,11) level for molecules A and B, and the CASPT2(18,15) level for molecules C and D.[b]

molecule A			molecule B			molecule C			molecule D		
State	E_{VA} (eV)	*f*	State	E_{VA} (eV)	*f*	State	E_{VA} (eV)	*f*	State	E_{VA} (eV)	*f*
T1 $^3(n_A\pi^*)$	3.14	-	T1 $^3(n_A\pi^*)$	3.16	-	T1	2.26	-	T1	2.45	-
T2 $^3(\pi_O\pi^*)$	3.28	-	S1 $^1(n_A\pi^*)$	3.37	-	T2 $^3(n_A\pi^*)$	3.12	-	T2 $^3(n_A\pi^*)$	3.12	-
S1 $^1(n_A\pi^*)$	3.34	-	T2 $^3(\pi_O\pi^*)$	3.44	-	T3 $^3(\pi_O\pi^*)$	3.27	-	S1 $^1(n_A\pi^*)$	3.34	-
T3	3.70	-	T3	3.73	-	T4	3.27	-	T3 $^3(\pi_O\pi^*)$	3.42	-
T4 $^3(n_B\pi^*)$	3.71	-	T4	3.80	-	S1 $^1(n_A\pi^*)$	3.31	-	T4	3.72	-
S2 $^1(n_B\pi^*)$	3.85	10^{-5}	S2 $^1(n_B\pi^*)$	3.96	-	T5	3.70	-	T5	3.73	-
T5	4.16	-	T5	4.33	-	S2 $^1(n_B\pi^*)$	3.83	10^{-5}	T6	3.89	-
T6	4.26	-	T6	4.38	-	T6	3.97	-	S2 $^1(n_B\pi^*)$	3.93	-
S3 $^1(L_b)$	4.37	10^{-3}	S3	4.57	10^{-4}	S3	4.20	0.150	S3 $^1(L_b)$	4.12	0.004
S4 $^1(L_a)$	5.02	0.235	S4	5.82	10^{-4}	S4	4.20	0.123	S4	4.88	0.001
S5 $^1(\pi_O\pi^*)$	5.68	0.025	S5	6.72	-	S5	4.34	0.143	S5	5.86	-

[a] The computed oscillator strengths (*f*) for the singlet-singlet transitions are also included.
[b] All the reported values refer to the corresponding ground state optimized geometry, $^1(gs)_{min}$.

3.3 Optimization of the triplet states and of the reactive $(T1/S0)_{mecp}$ STC

According to the assumed model, the photodegradation proceeds via population of the triplet $^3(\pi_O\pi^*)$ minimum, hereafter $^3(\pi_O\pi^*)_{min}$, that we have consequently characterized at the CASPT2(14,11)//CASSCF(10,8) level for molecules A and B and at the CASPT2(18,15)//CASSCF(14,12) level for molecules C and D. For the sake of completness, the energetically close triplet $^3(n_A\pi^*)$ state has also been analyzed. As the $^3(\pi_O\pi^*)$ and $^3(n_A\pi^*)$ states are the two lowest triplet states, we adopted a state-averaging over two roots with equal weight, for the calculations of both triplet and singlet states.

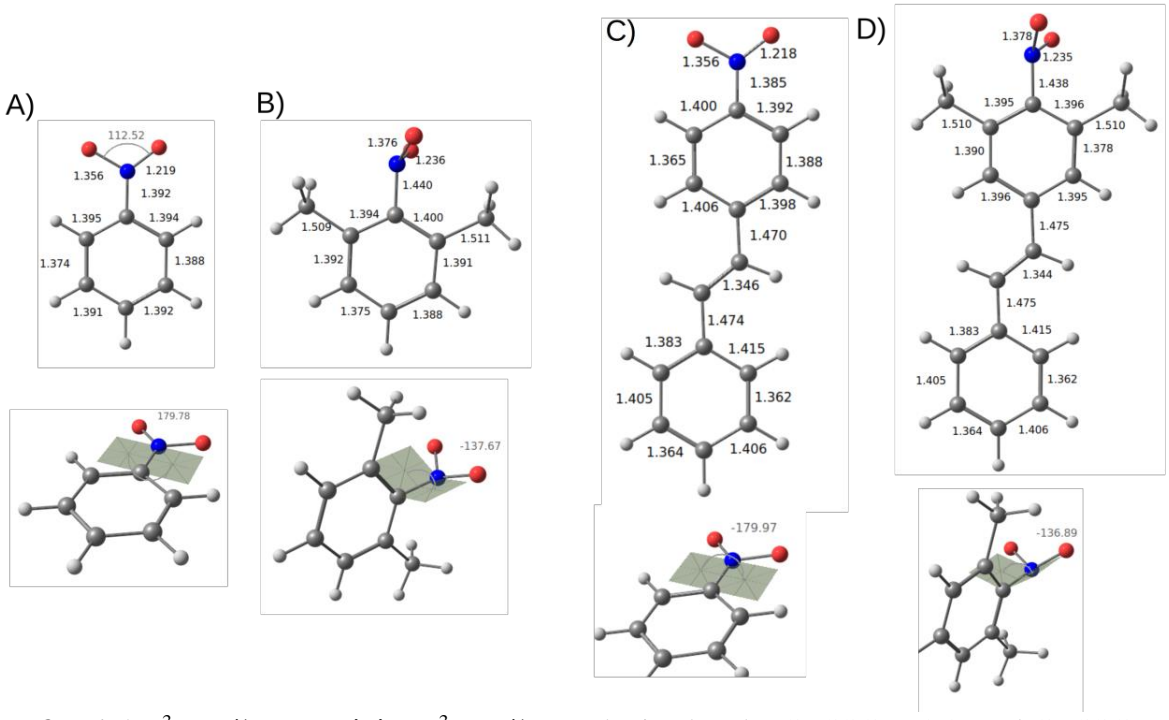

Figure 3. Triplet $^3(n_A\pi^*)$ state minima, $^3(n_A\pi^*)_{min}$, obtained at the CASSCF(10,8) and CASSCF(14,12) level for molecules A and B and for molecules C and D, respectively. Selected bond lengths (in Å) and angles (in degrees) are also reported. The lower panel shows the pyridimal angle of the NO_2 group.

The obtained minima for the $^3(n_A\pi^*)$ state, hereafter $^3(n_A\pi^*)_{min}$, are shown in Figure 3. As it is possible to observe, one common deformation with respect to the ground state minima is the elongation of one nitrogen-oxygen bond, with an increase of 0.121 and 0.120 Å for molecule A and C, and of 0.138 and 0.140 Å for molecule B and D. Another significant deformation with respect to the ground state minima is instead appering only for the dimethyl-substituted derivatives (i.e. molecules B and D) and not for molecules A and C: the nitro group of the former systems undergo a significant pyrimidalization, while in the latter molecules it keeps its planarity. The degree of such piramidalization can be observed in Figure 3, where the related dihedral angle is shown.

In order to confirm the nature of the obtained $^3(n_A\pi^*)_{min}$ minima, the corresponding frequencies have been computed. No negative frequencies were obtained for molecule B, one and two negative frequencies all lower than 100 cm^{-1} were obtained respectively for molecule A and C. Finally, at the $^3(n_A\pi^*)_{min}$ structure of molecule D two negative frequencies of 168.45 and 66.69 cm^{-1} have resulted (see Figure S5 in the SI).
The obtained minima for the $^3(\pi_O\pi^*)$ state, hereafter $^3(\pi_O\pi^*)_{min}$, are reported in Figure 4. Now we can observe that both nitrogen-oxygen bonds are significantly elongated with respect to their values at the corresponding $^1(gs)_{min}$ geometries, although of a lesser extend (0.068, 0.070, 0.067, and 0.071 Å for molecule A-D, respectively). Also, in these minima a pyramidalization of the nitro group of all four molecules is observed which is more pronunced for the dimethyl-substituted molecules. At the computed $^3(\pi_O\pi^*)_{min}$ geometries, no negative frequencies were obtained for molecules A and B, only a negative frequencies of 24 cm^{-1} for molecule C, and two two negative frequencis of 158.35 and 60.31 cm^{-1} for molecule D (see Figure S6 in the SI).

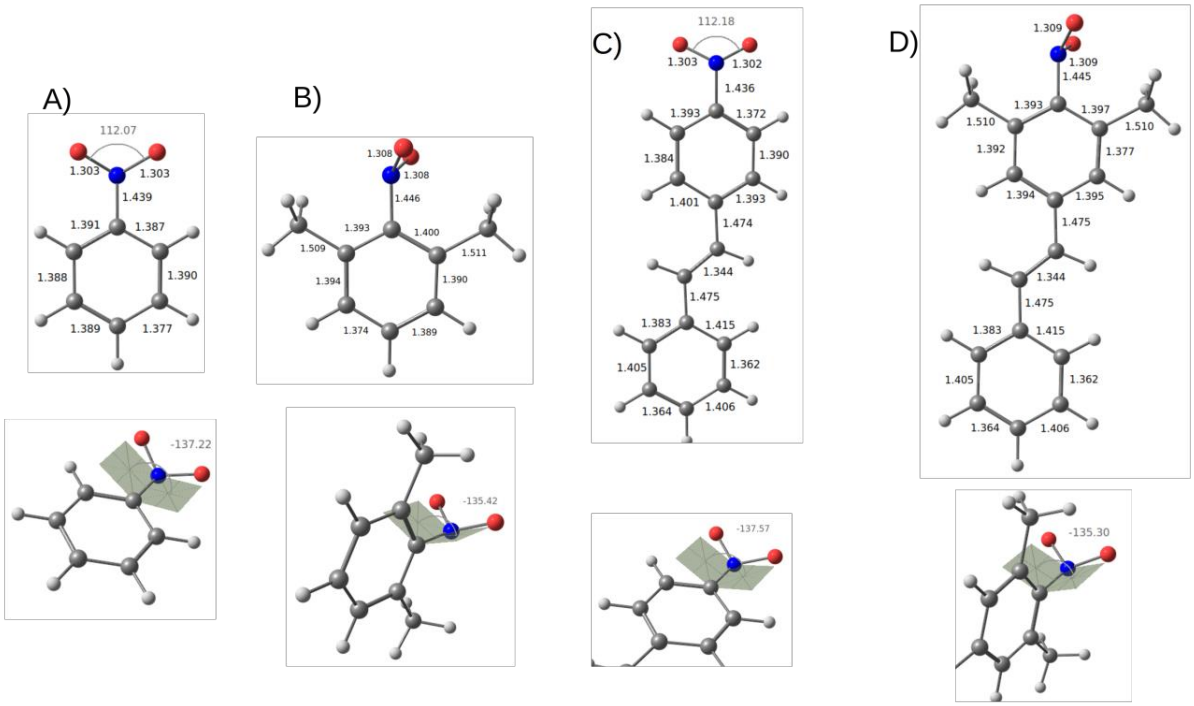

Figure 4. Triplet $^3(\pi_O\pi^*)$ state minima, $^3(\pi_O\pi^*)_{min}$, obtained at the CASSCF(10,8) and CASSCF(14,12) level for molecules A and B and for molecules C and D, respectively. Selected bond lengths (in Å) and angles (in degrees) are also reported. The lower panel shows the pyridimal angle of the NO_2 group.

A key geometry for the photoreaction leading to the formation of NO is the singlet-triplet crossing region characterized by the formation of an oxaziridine-like ring structure, from which the re-population of the ground state can evolve towards NO release. Starting with the STC previously obtained as a CASSCF(14,11) minimum energy crossing point for molecule A,[12] the corresponding reactive MECPs, hereafter $(T1/S0)_{mecp}$, have been computed for the here studied systems. The degeneracy of the T1 and S0 states at the obtained points have been verified at the CASPT2 level. The resulting MECPs are reported in Figure 5. As it can be observed, an oxaziridine-like ring structure is present in the four geometries. Once the described CASSCF critical points were obtained, their energies were recomputed at the CASPT2(14,11) and CASPT2(18,15) level for molecules A and B and for molecules C and D, respectively, and the results are collected in Table 3.

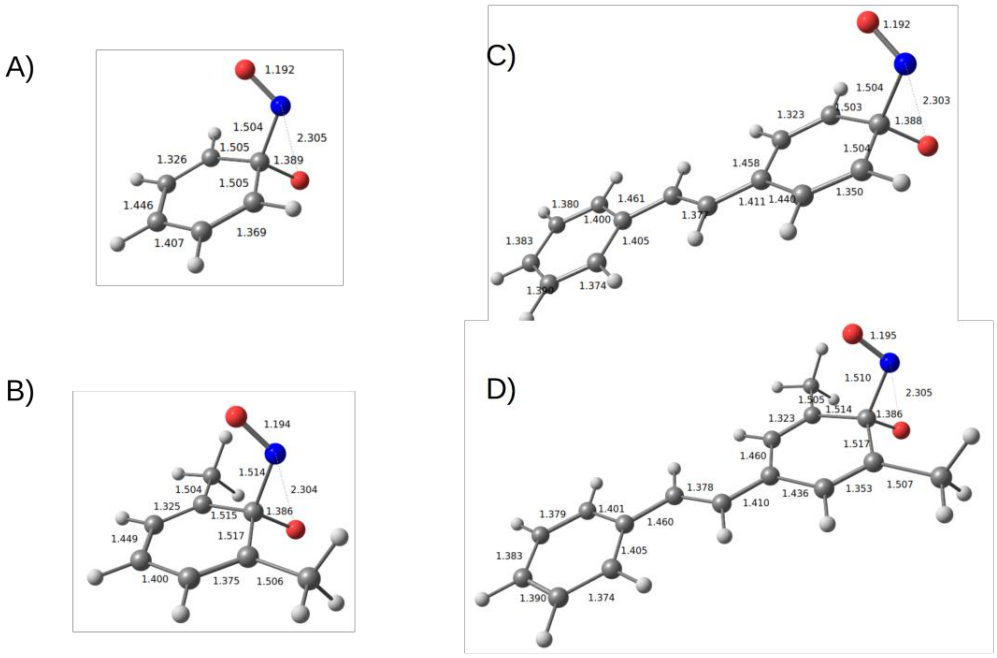

Figure 5. Reactive STC, $(T1/S0)_{mecp}$, obtained at the CASSCF(10,8) level for molecules A and B and and at the CASSCF(14,12) level for molecules C and D. Selected bond lengths (in Å) and angles (in degrees) are also reported.

Table 3. Energies (eV) of the low-lying singlet and triplet states at the optimized geometries. Energies computed at the CASPT2(14,11) level for molecules A and B, and at the CASPT2(18,15) level for molecules C and D.[a]

	molecule A			molecule B			molecule C			molecule D		
State Geometry	gs	$^3(\pi_O\pi^*)$	$^3(n_A\pi^*)$	gs	$^3(\pi_O\pi^*)$	$^3(n_A\pi^*)$	gs	$^3(\pi_O\pi^*)$	$^3(n_A\pi^*)$	gs	$^3(\pi_O\pi^*)$	$^3(n_A\pi^*)$
$^1(gs)_{min}$	0.00	3.40	3.35	0.00	3.56	3.76	0.00	3.39	3.35	0.00	3.56	3.31
$^3(n_A\pi^*)_{min}$	0.71	3.04	**2.88**	1.41	3.12	**3.27**	1.01	3.36	**3.40**	1.32	3.13	**3.11**
$^3(\pi_O\pi^*)_{min}$	1.08	**2.97**	2.87	1.25	**3.00**	3.16	1.25	**3.17**	3.05	1.21	**3.09**	2.93
$(T1/S0)_{mecp}$	3.67	**3.70**	4.21	3.65	**3.64**	4.04	3.56	**3.56**	3.75	3.20	**3.21**	3.64

[a] All the reported values refer to the corresponding ground state optimized geometry, $^1(gs)_{min}$.

3.4 Evaluation of the photodegradation path leading to NO

With the results of Table 3, we are in a position to evaluate the efficiency of the photodegradation paths leading to NO production according to the adopted model. The latter estimates the efficiency of the photoreaction on the basis of the energy barrier that the system has to surmount in order to reach the reactive STC from the triplet minimum. For nitrobenzene and nitronaphthalene the triplet minimum used to calculate this barrier was the $^3(\pi_O\pi^*)_{min}$ structure.[11,12] Since the $^3(n_A\pi^*)$ and $^3(\pi_O\pi^*)$ states have comparable energies, and in some cases the energy of $^3(n_A\pi^*)$ minimum is actually lower than the energy of the $^3(\pi_O\pi^*)$ minimum, and since the nature of the T1 state at the STC region is not clearly identifiable as the $^3(n_A\pi^*)$ or $^3(\pi_O\pi^*)$, we here decided to compute the barrier for reaching the STC

region from both triplet minima. The barrier is here evaluated as the energy difference between the triplet minima and the reactive STC. The results are presented in Table 4.

The energy barriers evaluated from both the $^3(n_A\pi^*)_{min}$ and $^3(\pi_O\pi^*)_{min}$ minima show a similar descending trend along the series of four molecules. According to that, both the addition of methyl groups and the extension of the π-conjugation would be expected to have a positive effect on the efficiency of the photodegradation process. In general the extension of the π-conjugation has a more pronounced effect that the addition of methyl groups. For example, the energy barrier for nitrobenzene from $^3(\pi_O\pi^*)_{min}$ diminishes by 0.44 eV when the π-system is enlarged (see values for molecules A and C) and by 0.09 eV with the methylation (see values for molecules A and B). Using the $^3(n_A\pi^*)_{min}$ minimum, larger differences are observed, but still the π-conjugation has a more prominent effect on the barrier that the presence of the methyls (0.66 and 0.45 eV reduction, respectively).

According to the data of Miyata and co-workers, the formation of NO for molecules B and C was not detected, while for molecule D a clear ESP signal was recorded as a result of the NO production. The theoretical model can be considered in agreement with the experimental behavior, since for molecule D the lowest energy barrier to reach the $(T1/S0)_{mecp}$ structure has been computed, equal to 0.10 and 0.12 eV when evaluated from the $^3(n_A\pi^*)_{min}$ and $^3(\pi_O\pi^*)_{min}$ minimum, respectively.

Table 4. Energy differences (eV) between $(T1/S0)_{mecp}$ and $^3(n_A\pi^*)_{min}$, and between $(T1/S0)_{mecp}$ and $^3(\pi_O\pi^*)_{min}$. Computations at the CASPT2(14,11)//CASSCF(10,8) and level for molecules A and B, and at the CASPT2(18,15)//CASSCF(14,12) level for molecules C and D.

$E[(T1/S0)_{mecp}] - E[^3(n_A\pi^*)_{min}]$			
molecule A	molecule B	molecule C	molecule D
0.82	0.37	0.16	0.10
$E[(T1/S0)_{mecp}] - E[^3(\pi_O\pi^*)_{min}]$			
molecule A	molecule B	molecule C	molecule D
0.73	0.64	0.29	0.12

3.5 Molecule E

From the results obtained here, a direct relation emerges between the ability of a nitroaromatic compound to photorelease NO and the energy separation between the triplet minima and the reactive STC. In order to confirm that, such an energy barrier has been evaluated for molecule E (see Figure 1), the system with the largest ability to photorelease NO among the molecules studied by Miyata and coworkers. If our model is correct, a low energy separation should be obtained.

The size and complexity of molecule E make its CASPT2//CASSCF description a challenging task. Dealing with the system as done for the previous molecules would mean performing CASSCF(16,14) optimizations and CASPT2(20,17) vertical calculations, since the second additional CC double bond requires the inclusion in the active space of the corresponding π and π* orbitals. Due to the high computational effort that such calculations will demand, we resort to a simplified approach focusing only on the $^3(\pi_O\pi^*)$ minimum and the reactive STC. In such a way, a first simplification was the computation of just one root, either S0 or T1, in all calculations.

In order to have a criterium for the reduction of the active space, we analyzed the results of molecule D, which is the most similar system to molecule E among the ones previously described. Looking in particular at states $^3(\pi_O\pi^*)$ and T1 in the CASSCF(18,15) vertical calculations performed at both the $^3(\pi_O\pi^*)$ minimum and the reactive STC of molecule D, it is possible to observe that three active orbitals have an occupation number larger than 1.95, meaning that their exclusion would in principle have little effect (see Figure S7 and S8 in the SI). To validate this, the $^3(\pi_O\pi^*)$ minimum and the reactive STC of molecule D have been re-characterized at the corresponding CASPT2(12,12)//CASSCF(12,12) level, this time working with only one root. The resulting geometries are comparable with the previously obtained (see Figure S9 in the SI) and, even more importantly, a similar energy separation between the triplet $^3(\pi_O\pi^*)$ minimum and the reactive STC is computed (0.13 eV) to the one obtained at the CASPT2(18,15)//CASSCF(14,12) level (0.12 eV).

Supported by this result, we decided to use a CAS(14,14) active space (i.e. the equivalent of the CAS(12,12) of molecule D plus the π/π^* orbitals on the additional CC double bond) for characterizing the $^3(\pi_O\pi^*)$ minimum and the reactive STC of molecule E. Indeed an energy separation of only 0.02 eV was obtained, further supporting the proposed direct relationship between this energy gap and the ability to photorelease NO.

Finally, we decided to evaluate the $(T1/S0)_{mecp}$/ $^3(\pi_O\pi^*)_{min}$ barrier using the reduced active space also for molecules A-C. That translates for molecule C into a CAS(12,12), while for molecules A and B into a CAS(8,8) active space. At all the new computed $^3(\pi_O\pi^*)_{min}$ minima, frequency calculations were performed. For molecules A and B no imaginary frequencies were obtained, while for molecules C-E two low imaginary frequencies result, equal to 48.42 and 24.61 cm^{-1}, 58.78 and 33.62 cm^{-1}, and 72.62 and 49.50 cm^{-1}, respectively. The obtained structures can thus indeed be considered as minima. This is particularly important for molecule D for which the CASSCF(14,12) $^3(\pi_O\pi^*)_{min}$ minimum described above displays a significant imaginary frequency of 158.35 cm^{-1}, and for molecule E, which has been characterized only with this level of theory. The corresponding results are presented in Table 5, and their analysis confirmed the conclusions drawn using to the data in Table 4. A schematic representation of the adopted model and the main result of the work is present in Figure 6.

Table 5. Energy difference (eV) between the $(T1/S0)_{mecp}$ and $^3(\pi_O\pi^*)_{min}$. Computations at the CASPT2(8,8)//CASSCF(8,8) level for molecules A and B, the CASPT2(12,12)//CASSCF(12,12) level for molecules C and D, and the CASPT2(14,14)//CASSCF(14,14) level for molecule E.

$E[(T1/S0)_{mecp}] - E[^3(\pi_O\pi^*)_{min}]$				
molecule A	molecule B	molecule C	molecule D	molecule E
0.77	0.56	0.27	0.13	0.02

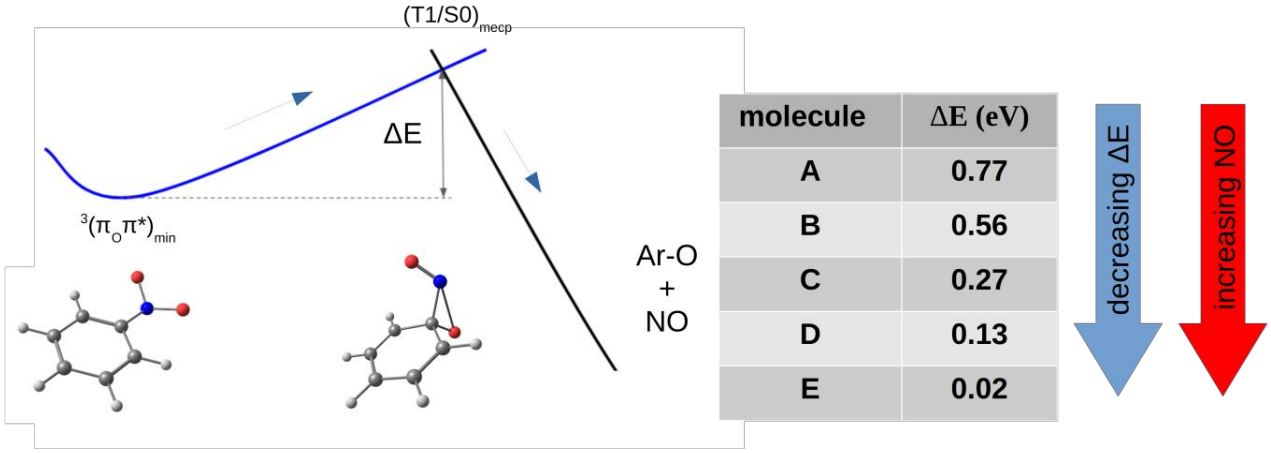

Figure 6. Schematic representation of the adopted model for the photodegradation leading to NO formation and trend of the energy barrier along the series of nitroaromatic compounds here studied.

Looking at the data of Table 5 and Figure 6, it is however true that the energies differences between the studied molecules are quite small, in particular regarding molecule D and E. It is consequently important to verify the consistency of the adopted method, especially considering the sensitivity of CASPT2//CASSCF results on the selected active space.[35,36] For this reason, we performed the following check. A linear-interpolation of internal coordinate (LIIC) path was obtained between each pair of $^3(\pi_O\pi^*)_{min}$ and $(T1/S0)_{mecp}$ structures whose energies are reported in Table 5. Starting from both the $^3(\pi_O\pi^*)_{min}$ and the $(T1/S0)_{mecp}$ critical points the energies along the LIIC were computed using as starting orbitals the one of the preceding structure. For example for molecule D, the same LIIC path has been computed starting from the $^3(\pi_O\pi^*)_{min}$ minimum and the CAS(12,12) space reported in Figure S7, and starting from $(T1/S0)_{mecp}$ point and the CAS(12,12) space reported in Figure S8. As shown in Table S1, S2 and in particular in Table S3, the energies of $^3(\pi_O\pi^*)_{min}$ and $(T1/S0)_{mecp}$ are indeed different depending on the starting orbitals used for computing the same LIIC. These differences are around 0.1 eV, being in the worst case of 0.22 eV and in the best case only 0.01 eV which shows that the strategy reported above for the reduction of the active space has resulted in slightly different active spaces for the $^3(\pi_O\pi^*)_{min}$ and $(T1/S0)_{mecp}$ structures. This is actually not very surprising, considering the clear different chemical connectivity characterizing the two of them. It is however significant that all three sets of data (i.e. the ones reported in Table 5, the ones obtained along the LIIC from $^3(\pi_O\pi^*)_{min}$, [Table S1], and the ones obtained along the LIIC from $(T1/S0)_{mecp}$, [Table S2]), indeed show the same trend, again supporting the proposed simple picture for the photorelease of NO in nitroaromatic compounds: the smaller the energetic separation between $^3(\pi_O\pi^*)_{min}$ and the $(T1/S0)_{mecp}$, the higher should be the photorelease efficiency of NO.

4. CONCLUSIONS

In the present contribution the photodegradation process leading to NO formation in a series of 5 nitroaromatic compounds of increasing complexity has been studied using the CASPT2//CASSCF protocol. Starting from nitrobenzene, four molecules have been derived through the addition of methyl groups at the ortho position with respect to the nitro group, and/or the enlargement of the π-conjugation. These systems have been chosen to analyze the effect that these structural modifications have on the photodegradation of nitrobenzene, as studied experimentally by Miyata and coworkers[4]. It

was assumed that in all systems the photodegradation proceeds via the same mechanism previously theoretically characterized for nitrobenzene and nitronaphthalene, for which the key point is the decay from the triplet minimum to a reactive STC region.[11,12]

The results of the calculations show a clear descending trend of the energy barrier to be crossed to reach the reactive STC along the series of nitroaromatic compounds. This result points to the fact that both the presence of methyl groups and the enlargement of the π-system favor the photoreaction. Looking in more detail at the computed barriers, it is possible to observe that the enlargement of the π-conjugation has a stronger effect than the methylation.

This scenario is in agreement with the experimental data of Miyata and coworkers, since the two molecules, D and E, for which NO formation was indeed detected, are here characterized by the lowest barriers for reaching the STC region. In particular molecule E, that in the mentioned experimental work resulted the system whose photodegradation is the most efficient, has the lowest computed energy barrier, of only 0.02 eV.

As a final point, it is important to highlight the main limitation of the present work. Here the energy barrier separating the triplet minimum and the STC region was evaluated as just the energy difference between the two critical points. A more rigorous approach will be the evaluation of the minimum energy path separating them, a task that at the moment, and mainly for computational reasons, was not performed. However the agreement with the available experimental results supports the validity of the adopted model and speak in favor of the proposed photodegradation mechanism.

Supplementary Material

Active space orbitals, figures of some optimized geometries, figures representing the imaginary frequencies, tables with the energies of the $^3(\pi_O\pi^*)_{min}$ and the $(T1/S0)_{mecp}$ structures obtained with different active spaces, and Cartesian coordinates of all e optimized geometries.

Acknowledgments

This project has received funding from the European Union's Horizon 2020 research and innovation programme under the Marie Sklodowska-Curie Grant Agreement No. 658173. This work has been supported by Projects PGC2018-099568-B-I00 and PID2021-128569NB-I00 and Excellence Unit María de Maeztu CEX2019-000919-M financed by MCIN/AEI/10.13039/501100011033/FEDER, UE, and the Generalitat Valenciana (PROMETEO/2020/077). G. W. also thanks the EPSRC (EP/V026690/1). A.G. thanks the MICINN for a "Juan de la Cierva Incorporación" postdoctoral grant (IJC2018-035123-I).

References

1 R. Atkinson, E. C. Tuazon, T. J. Wellington, S. M. Aschmann, J. Arey, A. M. Winer and J. N. Pitts, Atmospheric Chemistry of Aniline, N,N-Dimethylanillne, Pyridine, 1,3,5-Triazine, and Nitrobenzene, *Environ. Sci. Technol.*, 1987, **21**, 64–72.

2 T. B. Brill and K. J. James, Kinetics and Mechanisms of Thermal Decomposition of Nitroaromatic Explosives, *Chem. Rev.*, 1993, **93**, 2667–2692.

3 S. Sortino, Light-controlled nitric oxide delivering molecular assemblies, *Chem. Soc. Rev.*, 2010, **39**, 2903–2913.

4 T. Suzuki, O. Nagae, Y. Kato, H. Nakagawa, K. Fukuhara and N. Miyata, Photoinduced nitric oxide release from nitrobenzene derivatives, *J. Am. Chem. Soc.*, 2005, **127**, 11720–11726.

5 H. Nakagawa, K. Hishikawa, K. Eto, N. Ieda, T. Namikawa, K. Kamada, T. Suzuki, N. Miyata and J. I. Nabekura, Fine spatiotemporal control of nitric oxide release by infrared pulse-laser irradiation of a photolabile donor, *ACS Chem. Biol.*, 2013, **8**, 2493–2500.

6 D. B. Galloway, J. A. Bartz, L. G. Huey and F. F. Crim, Pathways and kinetic energy disposal in the photodissociation of nitrobenzene, *J. Chem. Phys.*, 1993, **98**, 2107–2114.

7 Y. He, A. Gahlmann, J. S. Feenstra, S. T. Park and A. H. Zewail, Ultrafast electron diffraction: Structural dynamics of molecular rearrangement in the NO release from nitrobenzene, *Chem. - An Asian J.*, 2006, **1**, 56–63.

8 W. Rodríguez-Córdoba, L. Gutiérrez-Arzaluz, F. Cortés-Guzmán and J. Peon, Excited state dynamics and photochemistry of nitroaromatic compounds, *Chem. Commun.*, 2021, **57**, 12218–12235.

9 M. F. Lin, Y. T. Lee, C. K. Ni, S. Xu and M. C. Lin, Photodissociation dynamics of nitrobenzene and o-nitrotoluene, *J. Chem. Phys.*, , DOI:10.1063/1.2435351.

10 M. L. Hause, N. Herath, R. Zhu, M. C. Lin and A. G. Suits, Roaming-mediated isomerization in the photodissociation of nitrobenzene, *Nat. Chem.*, 2011, **3**, 932–937.

11 A. Giussani, Toward the understanding of the photophysics and photochemistry of 1-nitronaphthalene under solar radiation: The first theoretical evidence of a photodegradation intramolecular rearrangement mechanism involving the triplet states, *J. Chem. Theory Comput.*, 2014, **10**, 3987–3995.

12 A. Giussani and G. A. Worth, Insights into the Complex Photophysics and Photochemistry of the Simplest Nitroaromatic Compound: A CASPT2//CASSCF Study on Nitrobenzene, *J. Chem. Theory Comput.*, 2017, **13**, 2777–2788.

13 K. J. Blackshaw, B. I. Ortega, N. K. Quartey, W. E. Fritzeen, R. T. Korb, A. K. Ajmani, L. Montgomery, M. Marracci, G. G. Vanegas, J. Galvan, Z. Sarvas, A. S. Petit and N. M. Kidwell, Nonstatistical Dissociation Dynamics of Nitroaromatic Chromophores, *J. Phys. Chem. A*, 2019, **123**, 4262–4273.

14 A. Giussani and G. A. Worth, Similar chemical structures, dissimilar triplet quantum yields: A CASPT2 model rationalizing the trend of triplet quantum yields in nitroaromatic systems, *Phys. Chem. Chem. Phys.*, 2019, **21**, 10514–10522.

15 A. Giussani and G. A. Worth, How important is roaming in the photodegradation of nitrobenzene?, *Phys. Chem. Chem. Phys.*, 2020, **22**, 15945–15952.

16 L. Saalbach, N. Kotsina, S. W. Crane, M. J. Paterson and D. Townsend, Ultraviolet Excitation Dynamics of Nitrobenzenes, *J. Phys. Chem. A*, 2021, **125**, 7174–7184.

17 O. L. Chapman, D. C. Heckert, J. W. Reasoner and S. P. Thackaberry, Photochemical Studies on 9-Nitroanthracene1, *J. Am. Chem. Soc.*, 1966, **88**, 5550–5554.

18 A. Giussani, M. Merchán, J. P. Gobbo and A. C. Borin, Relaxation mechanisms of 5-azacytosine, *J. Chem. Theory Comput.*, 2014, **10**, 3915–3924.

19 B. O. Roos, The complete active space SCF method in a fock-matrix-based super-CI formulation, *Int. J. Quantum Chem.*, 1980, **18**, 175–189.

20 K. Andersson, P. Å. Malmqvist and B. O. Roos, Second-order perturbation theory with a complete active space self-consistent field reference function, *J. Chem. Phys.*, 1992, **96**, 1218–1226.

21 D. Cremer, Møller-Plesset perturbation theory: From small molecule methods to methods for thousands of atoms, *Wiley Interdiscip. Rev. Comput. Mol. Sci.*, 2011, **1**, 509–530.

22 P. O. Widmark, P. Å. Malmqvist and B. O. Roos, Density matrix averaged atomic natural orbital (ANO) basis sets for correlated molecular wave functions - I. First row atoms, *Theor. Chim. Acta*, 1990, **77**, 291–306.

23 K. Pierloot, B. Dumez, P.-O. Widmark and B. O. Roos, Density matrix averaged atomic natural orbital (ANO) basis sets for correlated molecular wave functions, *Theor. Chim. Acta*, 1995, **90**, 87.

24 I. Fdez. Galván, M. Vacher, A. Alavi, C. Angeli, F. Aquilante, J. Autschbach, J. J. Bao, S. I. Bokarev, N. A. Bogdanov, R. K. Carlson, L. F. Chibotaru, J. Creutzberg, N. Dattani, M. G. Delcey, S. S. Dong, A. Dreuw, L. Freitag, L. M. Frutos, L. Gagliardi, F. Gendron, A. Giussani, L. González, G. Grell, M. Guo, C. E. Hoyer, M. Johansson, S. Keller, S. Knecht, G. Kovačević, E. Källman, G. Li Manni, M. Lundberg, Y. Ma, S. Mai, J. P. Malhado, P. Å. Malmqvist, P. Marquetand, S. A. Mewes, J. Norell, M. Olivucci, M. Oppel, Q. M. Phung, K. Pierloot, F. Plasser, M. Reiher, A. M. Sand, I. Schapiro, P. Sharma, C. J. Stein, L. K. Sørensen, D. G. Truhlar, M. Ugandi, L. Ungur, A. Valentini, S. Vancoillie, V. Veryazov, O. Weser, T. A. Wesołowski, P. O. Widmark, S. Wouters, A. Zech, J. P. Zobel and R. Lindh, OpenMolcas: From Source Code to Insight, *J. Chem. Theory Comput.*, 2019, **15**, 5925–5964.

25 N. Forsberg and P. Å. Malmqvist, Multiconfiguration perturbation theory with imaginary level shift, *Chem. Phys. Lett.*, 1997, **274**, 196–204.

26 T. B. Pedersen, F. Aquilante and R. Lindh, Density fitting with auxiliary basis sets from Cholesky decompositions, *Theor. Chem. Acc.*, 2009, **124**, 1–10.

27 F. Aquilante, L. De Vico, N. Ferré, G. Ghigo, P.-åke Malmqvist, P. Neogrády, T. B. Pedersen, M. Pitoňák, M. Reiher, B. O. Roos, L. Serrano-Andrés, M. Urban, V. Veryazov and R. Lindh, MOLCAS 7: The Next Generation, *J. Comput. Chem.*, 2010, **31**, 224–247.